Modeling of Drift Displacement of the Pellet Ablated Material for Outboard Side Injection in Large Helical Device

Akinobu MATSUYAMA, Florian KOECHL[1)], Bernard PÉGOURIÉ[2)], Ryuichi SAKAMOTO, Gen MOTOJIMA and Hiroshi YAMADA

National Institute for Fusion Science, Toki 509-5292, Japan
[1)]*Association EURATOM-ÖAW/ATI, Atominstitut, TU Wien, 1020 Vienna, Austria*
[2)]*CEA, IRFM, F-13108 Saint-Paul-lez-Durance, France*

(Received 10 November 2011 / Accepted 22 December 2011)

The outward drift displacement of the pellet ablated material is studied for low-field side injection in the Large Helical Device (LHD). Stopping of the drift acceleration is shown to be mainly due to the formation of an internal current circuit owing to helical variation of the magnetic field gradient. This process is the most efficient for stopping the cross-field motion of the ablatant in the LHD because, in helical configurations, the parallel scale length of the gradient variation is shorter than in tokamaks. Simulated ablation and deposition profiles are shown to compare well with the H_α emission and post-injection density and temperature profiles.

Keywords: pellet injection, ∇B-induced drift displacement, fueling efficiency, Large Helical Device

DOI: 10.1585/pfr.7.1303006

Pellet fueling [1, 2] has been considered as the most promising technique for fueling fusion reactors. It has the possibility to deposit the matter directly inside the last closed flux surface and allows to control the core and edge fueling properties independently. The efficiency of pellet injection is a critical issue regarding the plasma performance and the attainable fusion output in the reactors. Its optimization requires to develop a reliable modeling to gain confidence in extrapolation to the fueling of reactor-grade plasmas.

One of the major concerns related to pellet fueling is the shallow penetration of pellets injected into large devices, even at the highest velocity available with present-day technology. In tokamak experiments, this difficulty is partly overcome through high-field side (HFS) injection: in such a configuration, the pellet material, which ionizes rapidly after ablation, spontaneously penetrates into the core region of the plasma due to a drift directed down the magnetic field gradient. Due to this drift, HFS injected pellets can provide a better fueling efficiency, even at velocities less than 1 km/s. Conversely, in the case of the low-field side (LFS) injection, the degradation of the fueling efficiency has been observed, particularly with increasing additional power. As a whole, LFS/HFS injection experiments [3] in tokamaks have clearly demonstrated that the fueling efficiency of pellet injection depends essentially on the launching location, and thus the structure of the magnetic configuration.

The Large Helical Device (LHD) is a Heliotron device of the poloidal and toroidal period numbers $L = 2$ and $M = 10$, major radius $R = 3.6$–3.9 m, averaged minor radius $a = 0.6$ m, and magnetic field up to 3 T. In the LHD, pellets injected from the LFS at velocity $V_p \leq 1.2$ km/s have been routinely used to obtain high-density discharges sustained by the tangential neutral beam injection (NBI) heating. Previously, the physics of ablation in NBI-heated plasmas was studied for identifying some of the characteristics of pellet fueling in the LHD [4]. However, the post-ablation density build-up phase was not well understood, and the difference of fueling efficiency between LFS and HFS injected pellets is still unclear in non-tokamak geometries.

Recently, the drift displacement of the material deposited by LFS injected pellets have been identified in the LHD through the outward shift of the Δn_e^{exp} profile with respect to that of the H_α emission, where Δn_e^{exp} is the density increase following the pellet injection. The cross-field motion of the ablated material down the field gradient has also been directly observed by fast-imaging cameras [5]. Since this motion occurs on a timescale comparable to the homogenization time and much shorter than the diffusion time, it is suggested that the drift is of same origin as the $E \times B$ drift observed in tokamaks. In this letter, to interpret the experimental results, we adapt to the LHD geometry the pellet ablation-deposition code HPI2 [6] that takes into account the ∇B-induced drift displacement in axisymmetric tokamak geometry. For describing the cloud dynamics in nonaxisymmetric configuration, the effects of a helical field structure were newly included in the HPI2 code. In the following, simulation results are compared, for the first time, to experimental observations of LFS injected pellets

author's e-mail: matsuyama@LHD.nifs.ac.jp

in the LHD.

We begin with a description of the $E \times B$ drift model in an arbitrary magnetic configuration. The cross-field motion of the pellet cloud is due to the $E \times B$ drift associated to the polarization induced by the local gradient of the background magnetic field B_∞. We assume that the magnetic field generated by the pellet cloud itself, B_0, is much smaller than B_∞. In the following, the subscript '∞' denotes parameters of the background plasmas, whereas '0' denotes those of the pellet cloud. In early phase of the drift, the deposited material is accelerated down the magnetic field gradient, the evolution of the drift velocity $\boldsymbol{V}_\mathrm{d}$ being given by:

$$\frac{\mathrm{d}\boldsymbol{V}_\mathrm{d}}{\mathrm{d}t} = -\frac{2(p_0 - p_\infty)\nabla_\perp B_\infty}{n_0 m_\mathrm{i} B_\infty}, \tag{1}$$

where n_0 is the cloud density, m_i the ion mass, and p_0 and p_∞ the cloud and background-plasma pressures, respectively. Equation (1) shows that the drift acceleration is proportional to the pressure difference between the cloud and background plasma and to the inverse of the cross-field gradient scalelength $L_B = B_\infty/\nabla_\perp B_\infty$. Figure 1 shows schematically the variation of the magnetic field strength along the pellet path. At this location, the poloidal plasma cross section is horizontally elongated and the pellets are injected from the outboard side of the device (Fig. 1 (a)). The positive sign of $1/L_B$ in Fig. 1 (c) corresponds to the case where the pellet cloud drifts in the direction of increasing R, where the inverse of L_B in the outer region of the plasma (R = 4–4.5) is much larger than $1/R$. In tokamaks, L_B is, in first approximation, equal to the major radius R, and Eq. (1) reduces to the well-known expression of a drift-acceleration term proportional to $1/R$ [7]. Conversely, in non-axisymmetric devices, L_B is closer to the minor radius a. Therefore, the drift acceleration is expected to be larger in the LHD than what it would be in a tokamak of same aspect ratio.

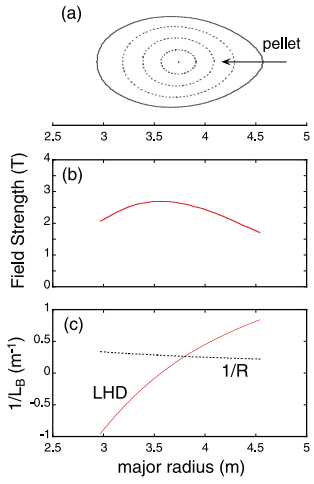

Fig. 1 Radial field gradient structure for outboard side injection in the LHD experiment.

However, the above picture - based on the evaluation only of the local $E \times B$ acceleration - is insufficient to describe the experimental behavior of the drift displacement. Mechanisms to reduce the cloud polarization need to be taken into account, and they were shown to be essential for the understanding of the ∇B-induced drift displacement [2]. In the HPI2 code, three mechanisms - whose relative importance depends on the structure of the magnetic configuration - are included which lead to a deceleration of the pellet cloud motion. They are: (1) on the Alfvén timescale, the depolarization due to the emission of Alfvén waves along the field lines from both ends of the cloud [6–9]; (2) on the collision timescale, the depolarization due to resistive currents flowing along the flux tubes that connect positively and negatively charged parts of the cloud, particularly in the vicinity of low-order rational surfaces [9] and (3) the averaging of the polarization along the cloud length due to the formation of an internal-current circuit simultaneously with the cloud parallel expansion [10, 11]. This latter effect, hereafter referred to as Rozhansky's effect, is illustrated for the LHD geometry in Fig. 2, showing how field lines inside the cloud close the circuit alimented by the ∇B particle drift, where they compensate the polarization charge by field-aligned internal currents.

Considering the most efficient deceleration mechanism in the case of shallow pellet penetration in the LHD, we put a particular emphasis on the third one. In the HPI2 code, the Rozhansky's effect is taken into account by a drift-damping factor $A[L_0]$ prior to the drift acceleration term. The latter is calculated through the averaging of the ∇B current over the length of the expanding cloud, along the field lines. One has then:

$$\frac{\mathrm{d}\boldsymbol{V}_\mathrm{d}}{\mathrm{d}t} = -A[L_0]\frac{2(p_0 - p_\infty)\nabla_\perp B_\infty}{n_\mathrm{i} m_0 B_\infty}. \tag{2}$$

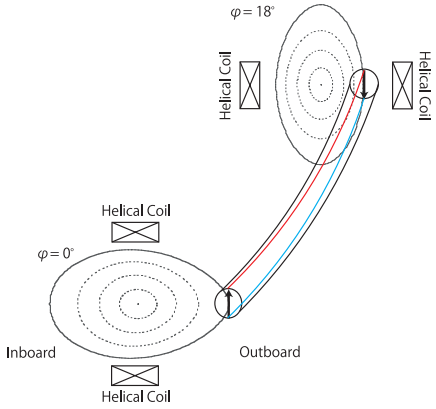

Fig. 2 Formation of the internal current circuit in the pellet cloud expanding over one toroidal period of the LHD. The parallel current flowing along the field lines in red and blue leads to the cancellation of the ∇B polarization at the cloud center ($\varphi = 0°$) with that at $\varphi = 18°$.

For tokamaks, a simple analytic model for $A[L_0]$ can be given as a function of the half-length of the cloud L_0:

$$A[L_0] = \frac{Rq}{L_0} \sin\left(\frac{L_0}{Rq}\right), \tag{3}$$

where q is the safety factor value. For generalizing this term, we use an expression of the ∇B current for an arbitrary magnetic configuration:

$$\boldsymbol{j}_{\nabla B} = \frac{2(p_0 - p_\infty)\boldsymbol{B}_\infty \times \nabla B_\infty}{B_\infty^3}. \tag{4}$$

Following an approach identical to that leading to the expression of Eq. (3) in the tokamak case, a general expression of the drift-damping factor is evaluated in terms of Eq. (4) as:

$$A[L_0] = \frac{1}{2L_0}\int_{-L_0}^{L_0} \frac{(\boldsymbol{B}_\infty \times \nabla B_\infty)/B_\infty^3 \cdot \boldsymbol{e}_\theta}{[(\boldsymbol{B}_\infty \times \nabla B_\infty)/B_\infty^3 \cdot \boldsymbol{e}_\theta]_{L_0=0}} \mathrm{d}l, \tag{5}$$

where $\boldsymbol{e}_\theta$ is a unit vector in the poloidal direction. In deriving Eq. (5), the parallel expansion along the field lines is assumed to be symmetric with respect to the cloud center, and the poloidal drift induced by the poloidal variation of the magnetic field is neglected. For circular tokamaks, it can easily be shown that Eq. (5) reduces to Eq. (3) if one assumes that the toroidal field is much stronger than the poloidal field. Equation (5) is therefore a straightforward generalization of the effect that is described by Rozhansky, *et al.* in Ref. [10].

To show main characteristics of the Rozhansky's effect, Fig. 3 shows how the drift-damping factor $A[L_0]$ varies with given lengths of the pellet cloud, showing the results (a) for the LHD and (b) for a tokamak of same aspect ratio. We here use a parabolic q profile for the tokamak: $q \sim 1.4$, 1.9 and 2.6 at $\rho = r_{\mathrm{eff}}/a = 0.5$, 0.7 and 0.9 (where r_{eff} is the averaged radius). In the LHD, the direction of the field gradient varies with rapid modulation, as does the field strength depending on the distance from the helical coils, and this dominates the stopping of the drift on the outer flux surfaces. As can be seen in the insert in Fig. 3 (a), even a relatively small toroidal extension of the cloud (whose characteristic scalelength is R/M) yields efficient damping, i.e., $A[L_0] < 1$ (note that, in all cases, $A[L_0 = 0] = 1$). Considering that the parallel expansion velocity ($V_\parallel$ = 10–100 km/s) is much faster than the cross-field drift velocity ($V_\mathrm{d} \lesssim 10$ km/s) [2], the characteristic timescale of the Rozhansky's effect, $\tau_R = R/(MV_\parallel)$, is seen to be comparable with the drift timescale $\tau_\mathrm{d} = a/V_\mathrm{d}$ in the LHD. In tokamaks, the corresponding τ_R expression is $qR/V_\parallel$, which is larger by more than one order of magnitude what it is in the case of the LHD (typically by a factor $\sim 1/M$). It is therefore much longer than τ_d, which explains why the Rozhansky's effect has only a moderate effect on the deceleration of the deposited cloud in tokamaks as compared to its importance in the LHD (see Fig. 3 (b)).

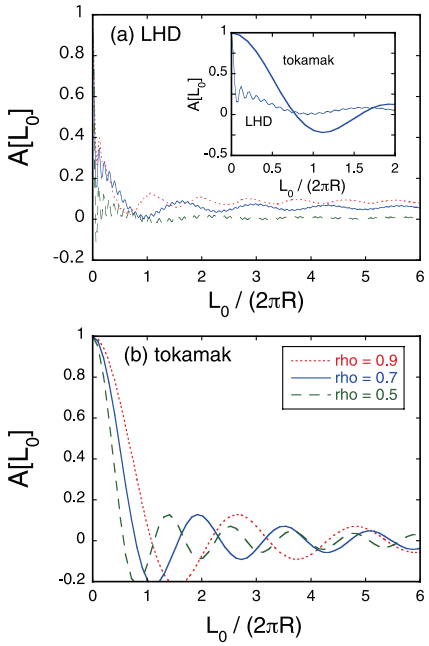

Fig. 3 Comparison of the drift-damping factor $A[L_0]$ at different radial location of the pellet cloud: (a) LHD with R_{ax} = 3.75 m and (b) tokamak of same aspect ratio.

We have implemented Eq. (5) instead of Eq. (3) into the HPI2 code for evaluating the Rozhansky's effect in a helical magnetic field structure. We also introduced the other magnetic-field related parameters specific to the LHD, such as the q profile and magnetic shear. Although our model can in principle be applied to a full 3-D equilibrium, only the dominant toroidal and helical variations of B_∞ are taken into account in the present work. The HPI2 simulation consists in two part: (1) the ablation calculation which evaluates the local source of particles along the pellet path and the penetration depth for given plasma profiles [12], and (2) the homogenization calculation which evaluates in a consistent way the cross-field drift and parallel expansion of the cloud in a four-fluids Lagrangian approximation [6]. In the present work, the heat source term associated to the fast ion population due to tangential NBI was included in the ablation calculation, but not yet in that of the cloud expansion. This simplification is still reasonable for shallow pellet penetration in case of central NBI heating, because the thermal electron heat flux is much larger than the fast-ion one in the outer region of the plasma.

A comparison between the HPI2 prediction and the measurements is presented in Fig. 4 in the case of a pellet injected into low-density target plasma with tangential NBI heating. Main parameters are a pellet particle content $N_\mathrm{p} = 8.8 \times 10^{20}$ atoms (nominal), injection velocity $V_\mathrm{p} = 1.2$ km/s, heating power $P_{\mathrm{NBI}} = 4.8$ MW, electron temperature and density $T_{\mathrm{e}\infty}(\lambda_\mathrm{p}^{\mathrm{exp}}) = 1.6$ keV and $n_{\mathrm{e}\infty}(\lambda_\mathrm{p}^{\mathrm{exp}}) = 6.9 \times 10^{18}$ m^{-3}, where $\lambda_\mathrm{p}^{\mathrm{exp}}$ is the experimental penetration depth. The experimental penetration was estimated from the pellet velocity and duration of the H_α

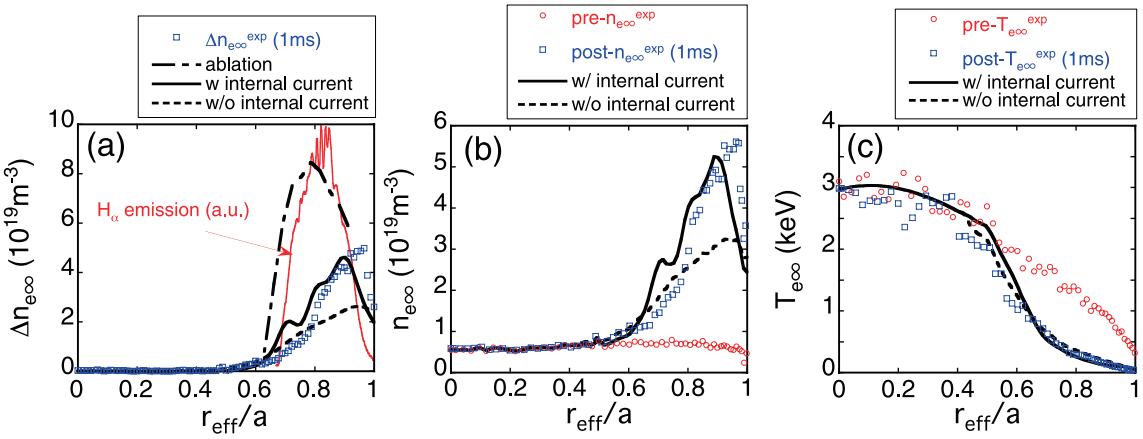

Fig. 4 Comparison between measurements and code prediction for the LHD discharge no. 103396: (a) ablation and deposition profiles, the H_α emission (a.u.), and $\Delta n_{e\infty}$ profile; (b) pre- and post-$n_{e\infty}$ and (c) pre- and post-$T_{e\infty}$ profiles.

emission, whereas the particle deposition from Thomson scattering measurements recorded 1 ms after the time of the begininng of ablation (identified by the increase in H_α emission). Figure 4 shows a comparison between the HPI2 simulation and the experiment: (a) ablation and deposition profiles, (b) electron density, and (c) electron temperature profiles before and after the injection. Using the pre-injection $T_{e\infty}$ and $n_{e\infty}$ profiles, the simulation predicts the pellet to penetrate up to $\rho \sim 0.63$, which compares well with the value $\rho \sim 0.67$ obtained from the duration of the H_α line emission, as shown in Fig. 4 (a). The location of the maximum of ablation in our simulation, at $\rho \sim 0.78$, is also seen to agree with that of the H_α emission peak at $\rho \sim 0.8$–0.85. In the absence of ∇B-induced displacement, the particle deposition would correspond to the dashed-dotted curve in Fig. 4 (a), exhibiting a maximum $\Delta n_{e\infty} = 8.46 \times 10^{19}\,\mathrm{m}^{-3}$ at $\rho \sim 0.78$. But experimentally, the density profile measured 1 ms after ablation shows that the deposition profile is shifted outwardly, which displays a maximum $\Delta n_{e\infty}^{\mathrm{exp}} = 4.98 \times 10^{19}\,\mathrm{m}^{-3}$ at $\rho \sim 0.97$. This is in good agreement with the solid curve in Fig. 4 (a), which is the deposition profile calculated when taking into account the drift displacement, showing a maximum $\Delta n_{e\infty} = 4.6 \times 10^{19}\,\mathrm{m}^{-3}$ at $\rho \sim 0.9$. For comparison, the dashed curve is the deposition prediction when the Rozhansky's effect is neglected (i.e., using $A[L_0] = 1$), showing a significant overestimation of the outward displacement. In Figs. 4 (b) and (c), a good agreement between measurements and simulation results is also shown for the post-injection $n_{e\infty}$ and $T_{e\infty}$ profiles when all the drift-damping effects are taken into account.

The fueling efficiency is defined as the ratio of the amount of particles deposited in the confined plasma with the pellet initial content, where we used the last-closed flux surface of the vacuum magnetic configuration to define the boundary for low-β plasma. From Fig. 4, it was evaluated in both the simulated and experimental cases for shallow penetration LFS injected pellets, yielding 58% and 55%, respectively. When neglecting the Rozhansky's drift-damping factor ($A[L_0] = 1$, dashed curves in Fig. 4), a fueling efficiency of 40% is obtained, showing a significant overestimation of the experimental loss rate of the pellet material. It follows that about 40–50% of the fueled particles are lost from the confinement region due to the ∇B-induced displacement, which has therefore a significant impact on the fueling efficiency of LFS injected pellets, as in the case of tokamaks.

In this letter, a drift model for pellets injected in the LHD was described in the same framework as that used in the case of tokamak modeling. Hence, the present study provides potentially a common physical picture of pellet fueling for both tokamaks and helical devices. A comparison between different magnetic configurations can improve our quantitative understanding of the influence of magnetic field structure on the pellet deposition and associated fueling efficiency. In a subsequent work, the simulation will be applied to various experimental conditions to increase the capability of the code to identify the characteristics of the pellet fueling in the LHD.

The authors acknowledge support by the LHD experiment group. This work was supported by NIFS10ULPP004, by the Grants-in-Aid for Research Activity Start-Up by the Japan Society for Promortion of Science (JSPS), and by the Grants-in-Aid Scientific Research (S) by the Ministry of Education, Culture, Sports, Science and Technology.

[1] S.L. Milora *et al.*, Nucl. Fusion **35**, 657 (1995).
[2] B. Pégourié, Plasma Phys. Control. Fusion **49**, R87 (2007).
[3] P.T. Lang *et al.*, Phys. Rev. Lett. **79**, 1487 (1997).
[4] M. Hoshino *et al.*, Plasma Fusion Res. **1**, 033 (2006).
[5] R. Sakamoto and H. Yamada, Plasma Fusion Res. **6**, 1402085 (2011).
[6] B. Pégourié *et al.*, Nucl. Fusion **47**, 44 (2007).
[7] P.B. Parks, W.D. Sessions and L.R. Baylor, Phys. Plasmas **7**, 1968 (2000).

[8] A.R. Polevoi and M. Shimada, Plasma Phys. Control. Fusion **43**, 1525 (2001).
[9] N. Commaux *et al.*, Nucl. Fusion **50**, 025011 (2010).
[10] V.A. Rozhansky *et al.*, Plasma Phys. Control. Fusion **46**, 575 (2004).
[11] I. Yu. Senichenkov *et al.*, Nucl. Fusion **46**, 788 (2006).
[12] B. Pégourié *et al.*, Plasma Phys. Control. Fusion **47**, 17 (2005).